The Mechanism of Extracellular Stimulation of Nerve Cells on an Electrolyte-Oxide-Semiconductor Capacitor

Ingmar Schoen and Peter Fromherz
Department of Membrane and Neurophysics, Max Planck Institute for Biochemistry, Martinsried/Munich, Germany

ABSTRACT Extracellular excitation of neurons is applied in studies of cultured networks and brain tissue, as well as in neuroprosthetics. We elucidate its mechanism in an electrophysiological approach by comparing voltage-clamp and current-clamp recordings of individual neurons on an insulated planar electrode. Noninvasive stimulation of neurons from pedal ganglia of *Lymnaea stagnalis* is achieved by defined voltage ramps applied to an electrolyte/HfO_2/silicon capacitor. Effects on the smaller attached cell membrane and the larger free membrane are distinguished in a two-domain-stimulation model. Under current-clamp, we study the polarization that is induced for closed ion channels. Under voltage-clamp, we determine the capacitive gating of ion channels in the attached membrane by falling voltage ramps and for comparison also the gating of all channels by conventional variation of the intracellular voltage. Neuronal excitation is elicited under current-clamp by two mechanisms: Rising voltage ramps depolarize the free membrane such that an action potential is triggered. Falling voltage ramps depolarize the attached membrane such that local ion currents are activated that depolarize the free membrane and trigger an action potential. The electrophysiological analysis of extracellular stimulation in the simple model system is a basis for its systematic optimization in neuronal networks and brain tissue.

INTRODUCTION

Extracellular stimulation of nerve cells in a tissue is a classical technique in brain research and a fundamental tool in neuroprosthetics (1–3). Electrical current that originates at an electrode creates a gradient of extracellular electrical potential such that an action potential may be elicited. Possible depolarizing and hyperpolarizing effects on different parts of oriented nerve cells with dendrite, soma, and axon were pointed out (4), and were simulated in a theoretical model (5). In recent years, particular attention was given to the extracellular stimulation of cultured neurons on planar metallic electrodes (6–9). Questions considered were: Which part of a neuron is responsible for excitation? What is the role of anodic and cathodic current on attached and nonattached parts of the membrane? What is the contribution of capacitive and of Faradayic current? Are defined currents or defined voltages better to control stimulation?

In a tissue as well as in a dish with cultured neurons, the geometry of numerous cells with a meshwork of dendrites and axons is rather involved such that an electrophysiological characterization of extracellular stimulation is not possible. Furthermore, with common metal electrodes it is difficult to avoid Faradayic currents that give rise to toxic electrochemical reactions. For these reasons, we present here an electrophysiological study of extracellular stimulation in a model system under simple and well-defined conditions:

1. We use an insulated planar electrode without Faradayic current.
2. We study neurons that are attached to the electrode without branched dendrites and axons.
3. We apply stimulation by defined voltages with rising ramps as well as falling ramps to provide anodic and cathodic stimulation.
4. We compare extracellular stimulation in a whole-cell patch-clamp configuration for voltage-clamp and for current-clamp.

The cell-electrode geometry is sketched in Fig. 1 *A*. The attached domain of the plasma membrane is separated from the insulated electrode by a thin layer of electrolyte whereas the free domain is in contact to the bath. Capacitive current across the electrode/electrolyte interface gives rise to a profile of extracellular voltage in the area of adhesion and to a change of the intracellular voltage with respect to the bath on ground potential. A patch-pipette is used to record the response of the neuron—the membrane current under voltage-clamp and the membrane voltage under current-clamp. Under these conditions, we are able to elucidate the effect of extracellular stimulation on the voltage-gated ion channels in the attached as well as in the free domain of the membrane and also the role of gating in either domain for the elicitation of an action potential.

As an electrode we choose an electrolyte/oxide/silicon capacitor. The insulating material is hafnium oxide (10), a high κ dielectric used in nanoelectronic devices (11). The Faradayic current is negligible for a wide range of voltages. The capacitance is distinctly higher as compared to SiO_2 that was used in earlier experiments on neuron-silicon interfacing (12–14). Nonetheless, it is far lower than with metal electrodes. To compensate for the rather low capacitive current,

Submitted August 7, 2006, and accepted for publication October 19, 2006.

Address reprint requests to Peter Fromherz, Tel.: 49-89-8578-2820; E-mail: fromherz@biochem.mpg.de.

0006-3495/07/02/1096/16 $2.00

doi: 10.1529/biophysj.106.094763

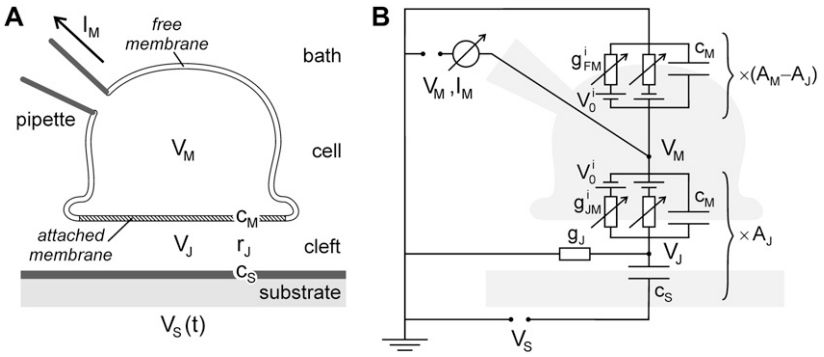

FIGURE 1 Nerve cell on a capacitor and two-domain-stimulation (TDS) model. (*A*) Schematic view, not to scale. The cell diameter is ~50 μm, the width of the cleft between cell and chip is ~20 nm. Two domains of the plasma membrane are distinguished, an attached domain with area A_J (*shaded*) in contact to the capacitor and a free domain with area A_M–A_J in contact to the bath. A voltage ramp $V_S(t)$ applied to the substrate induces an extracellular voltage V_J in the cell-capacitor junction. The resulting change of the intracellular voltage V_M and the membrane current I_M are measured or controlled with a pipette. (*B*) Equivalent circuit of TDS model. Substrate, cell-chip contact, membrane in the junction (JM) and free membrane (FM) are characterized by the area-specific parameters of substrate capacitance c_S, of membrane capacitance c_M, of seal conductance g_J, and of ionic conductances g^i_{JM} and g^i_{FM} (reversal voltages V^i_0). The parameters of the junction are weighted by the area A_J and the parameters of the free membrane by the area A_M-A_J as indicated.

we use large nerve cells from *Lymnaea stagnalis*. By suitable preparation (15) and proper timing of the experiment, a large and tight contact is achieved between capacitors and cells without arborized neurites.

This article is organized as follows. After a section on Materials and Methods, we summarize basic relations of capacitive stimulation under voltage-clamp and current-clamp in terms of a two-domain-stimulation (TDS) model. That chapter serves as a basis for a planning of the experiments and for their interpretation. Then we describe the capacitive polarization of neurons under current-clamp for closed ion channels. Under voltage-clamp, the gating of ion channels in the attached membrane is considered as it is induced by falling voltage ramps. For comparison, the gating of all channels is characterized by variation of the intracellular voltage. Finally, action potentials are elicited under current-clamp by applying falling as well as rising voltage ramps. The mechanism of stimulation is interpreted in terms of the results of capacitive polarization under current-clamp and of the ionic currents under voltage-clamp.

MATERIALS AND METHODS

Chips

We use electrolyte/oxide/silicon capacitors as described in a previous study (10). Quadratic 4 × 4 mm chips were made of p^+-doped silicon (0.01 Ωcm) with a 1-μm-thick SiO_2 field oxide. Circular capacitors with a diameter of 250 μm are obtained by etching and insulation with 10 nm HfO_2 by atomic layer deposition. The area-specific capacitance in electrolyte is $c_S = 1.22$ $\mu F/cm^2$ in the accumulation region of silicon beyond a voltage of $V_s = 2$ V between Si and Ag/AgCl without leakage current up to $V_s = 4.5$ V. An aluminum layer (200 nm) is evaporated on the back.

We glue the chips on an aperture in the bottom of 35 mm polystyrene culture dishes (Falcon 3001, Becton Dickinson, NJ) and contact them with gilded springs. They are cleaned with hot detergent (5% Tickopur R36, Bandelin, Berlin, Germany), rinsed with Millipore water (Millipore, Billerica, MA), dried in nitrogen and sterilized with UV light for 20 min. They are coated with the laminin fragment YIGSR (16) (No. C-0668, Sigma, Taufkirchen, Germany) by adsorption from a 0.5 mg/ml solution in 10% (v/v) acetic acid for 2 h.

Nerve cells

The isolation of nerve cells from *Lymnaea stagnalis* follows the procedure described by Syed et al. (15). The central ring of ganglia is isolated from snails with a shell length of ~15 mm. After digestion with trypsin (No. T-4665, Sigma; 50 U/3 ml, 20 min at 18°C) and inhibition of the enzyme with soybean inhibitor (No. T-9003, Sigma, 2 mg/ml, 10 min) the tissue around the pedal ganglia is removed. Neuronal somata with parts of the axonal processes are extracted from the A-clusters with a suction pipette (75 μm diameter) attached to a syringe (1750LT, 500 μl, Hamilton, Bonaduz, Switzerland) with a polyethylene tubing. The isolated neurons are kept in defined medium (DM) (18°C, 80% humidity) with plastic dishes coated by adsorption of bovine serum albumin (No. A-9647, Sigma, 3 mg/ml) for 1 h in normal saline (NS). There the axon stump degenerates, leaving an approximate spherical cell body. After one day, the neurons are transferred to a chip with 2 ml DM and placed on the capacitor. DM is made by mixing Leibovitz's L-15 medium with fourfold concentration (without inorganic salts and without L-glutamine, special order, No. 21083027, Invitrogen, Karlsruhe, Germany) and from normal *Lymnaea* saline (NS) (40 mM NaCl, 1.7 mM KCl, 1.5 mM $MgCl_2$, 4.1 mM $CaCl_2$, 10 mM HEPES, pH 7.6 adjusted with NaOH) with fourfold concentration at a ratio 1:1 by dilution with Milli-Q water (Millipore) to final concentrations and supplementing with 25 μg/ml gentamycin sulfate. All reagents were from Sigma unless mentioned otherwise.

Cell-chip adhesion

Chips with neurons are mounted in a microscope (BX50WI, Olympus, Hamburg, Germany) with a differential interference contrast (DIC) inset. The cells are cultured for 1–4 h until the visible adhesion area becomes similar to the diameter of the somata. The distance between chip and attached cell membrane is measured by fluorescence interference contrast (FLIC) microscopy with the hemicyanine dye $DiIC_{18}(3)$ as a fluorescent probe (17). Common silicon chips with SiO_2 terraces are used because FLIC chips with HfO_2 were not available. Cleaning and coating of the FLIC chips follows the protocol for the stimulation chips.

Electrical measurements

We perform experiments at 23 ± 2°C with patch-clamp pipettes in whole-cell configuration to provide for defined extra- and intracellular conditions and also with impaled sharp micropipettes to avoid a washout of cytosolic factors.

The sharp micropipettes are pulled (DMZ Universal puller, Zeitz-Instruments, Martinsried, Germany) from borosilicate glass (TW150F, WPI, Sarasota, FL), filled with saturated K_2SO_4 and contacted with chlorinated

silver wires. The experiments are carried out in DM that contains 4.1 mM Ca^{2+}. The bath is held at ground potential with a Ag/AgCl electrode (EP05, WPI). The resistances are in the range of 35–60 MΩ. Current-clamp experiments are performed with a bridge amplifier (BA-1S, NPI Electronic, Tamm, Germany).

Micropipettes are pulled from borosilicate glass (GB150T-10, Science Products, Hofheim, Germany) with a three-stage puller (DMZ Universal puller, Zeitz-Instruments) and fire-polished. They are coated with Sylgard (Dow Corning, Midland, MI) and filled with an intracellular solution (ICS) containing 6 mM NaCl, 31 mM KCl, 20 mM KF, 5 mM HEPES, 5 mM EGTA (pH 7.6 adjusted with KOH). DM is replaced by an extracellular recording solution (ECS) without Ca^{2+} containing 40 mM NaCl, 1.7 mM KCl, 5.6 mM $MgCl_2$, 0.2 mM $CdCl_2$, 10 mM HEPES (pH 7.6 adjusted with NaOH, specific resistivity $\rho_E = 163\ \Omega$cm). An ECS for control experiments without potassium and sodium currents contains 65 mM TEA chloride, 1.5 mM $MgCl_2$, 5 mM HEPES, 5 mM EGTA (pH 7.6 adjusted with KOH, specific resistivity $\rho_E = 165\ \Omega$cm). ECS and ICS are adjusted to an osmolality of ~140 mmol/kg with D^+ glucose. The resistances of the pipettes are in the range of 1.7–2.2 MΩ. Seals are obtained by suction (20 cm water column) for 20 s. After breakthrough by strong suction, the serial resistance is compensated by >70%. Cells are discarded when the seal resistance is <500 MΩ and when the serial resistance is >4 MΩ. Data are recorded with an EPC8 patch-clamp amplifier (HEKA Electronics, Lambrecht, Germany), and filtered at 3 kHz. In some voltage-clamp experiments, a P/4 protocol is used to subtract capacitive and leak currents.

For capacitive stimulation, voltage ramps (waveform generator 33120A, Agilent, Palo Alto, CA) are applied between the chip and the Ag/AgCl electrode in the bath. To determine the capacitive current, the voltage drop at a serial 50 Ω resistor is recorded.

TWO-DOMAIN-STIMULATION MODEL

Usually the interpretation of electrophysiological experiments relies on three concepts:

1. The electrical potential is constant across the cytoplasm and across the bath.
2. The difference of the two electrical potentials—the membrane voltage—is given by the voltage between two Ag/AgCl electrodes in the cytoplasm and in the bath.
3. The current through all domains of the membrane is driven by the same membrane voltage.

In a situation of extracellular stimulation these assumptions are no longer valid. Current from the stimulation electrode to the bath electrode gives rise to a gradient of the electrical potential in the extracellular electrolyte that depends on the geometry of cell and stimulation electrode as well as on the resistivity of the bath. Even though the cytoplasm may still be isopotential, the membrane voltage depends on the position of the membrane domain in the field of the extracellular potential. Thus the current through different membrane domains is controlled by different voltages.

In the special case of cell adhesion on a planar electrode, we may distinguish

1. The region of adhesion with a large drop of the electrical potential due to the high electrical resistance of the narrow cleft between cell and electrode, and
2. The region in the surround of the cell with a minor drop of the electrical potential in the surrounding bath.

As a basis for the planning of the experiments and for the discussion of the results, we introduce a two-domain-stimulation (TDS) model that relies on two approximations:

1. The minor drop of the electrical potential in the surround of the cell above the uncovered capacitor is neglected. The extracellular electrical potential near the free membrane is assumed to be probed by the bath electrode.
2. The potential profile in the area of adhesion is replaced by a mean extracellular potential. There exists a potential difference—an extracellular voltage—between the attached membrane and the bath. Hence the current through the attached membrane is driven by a different voltage as compared to the current through the free membrane.

Deviations between the TDS model and the experimental data may occur if these assumptions are not perfectly valid.

Neuron-capacitor system

We consider an individual nerve cell on oxidized silicon. The attached plasma membrane is separated from the substrate by a thin film of electrolyte as illustrated in Fig. 1 *A*. The contact area with the insulating layers of membrane and oxide forms a planar core-coat conductor (14,18). When a changing voltage V_S is applied to the substrate with an area-specific capacitance c_S, current flows along the cell-chip junction with a sheet resistance r_J and across the membrane with an area-specific capacitance c_M. A profile of extracellular voltage V_J arises in the junction as well as a change of the intracellular voltage V_M with respect to the bath at ground potential. A drop of extracellular voltage in the surround of the cell with respect to the bath is neglected.

To account for crucial features of capacitive stimulation, we use a model that describes the core-coat conductor as a single equipotential compartment (12,14,18,19) with a representative extracellular voltage V_J as illustrated in Fig. 1 *B*. We distinguish two domains of the membrane with a total area A_M: the free membrane with an area A_M–A_J is controlled by the voltage V_M, whereas the attached membrane with an area A_J and a fraction $\alpha_{JM} = A_J/A_M$ is controlled by the voltage V_M–V_J.

The two-compartment stimulation (TDS) model is determined by the capacitance $(A_M–A_J)c_M$ and the ionic conductances $(A_M–A_J)g^i_{FM}$ of the free membrane and the capacitance A_Jc_M and ionic conductances $A_Jg^i_{JM}$ of the attached membrane (area-specific conductances g^i_{FM} and g^i_{JM}), as well as by the chip capacitance A_Jc_S in the junction and the conductance A_Jg_J from the junction to the bath. The area-specific conductance $g_J = \eta_J/r_JA_J$ is defined in terms of the sheet resistance, the contact area, and a geometry factor that is $\eta_J = 8\pi$ under stationary conditions and $\eta_J = 5.78\pi$ for relaxation (see Appendix).

Passive response to voltage ramps

Without ionic membrane conductances ($g^i_{JM} = g^i_{FM} = 0$), the balance of electrical current in the cell and in the cell-chip

junction is expressed by Eqs. 1 and 2 where I_M is the net membrane current through a pipette:

$$(A_M - A_J)c_M\frac{dV_M}{dt} + A_J c_M\frac{d(V_M - V_J)}{dt} = I_M, \quad (1)$$

$$A_J c_M\frac{d(V_J - V_M)}{dt} + A_J g_J V_J = A_J c_S\frac{d(V_S - V_J)}{dt}. \quad (2)$$

When we apply a voltage ramp with constant slope $\Delta V_S/\Delta t_S$ to the capacitor under current-clamp with $I_M = 0$, an extracellular voltage V_J is induced as well as voltage changes ΔV_M and $\Delta V_{JM} = \Delta(V_M - V_J)$ across the free and attached membrane. After the onset of a ramp at $t = 0$, we obtain Eqs. 3 and 4 with a stationary extracellular voltage $V_J^\infty = (c_S/g_J)\Delta V_S/\Delta t_S$ and a time constant $\tilde{\tau}_J = (\tilde{c}_M + c_S)/g_J$, where $\tilde{c}_{JM} = c_M(1 - \alpha_{JM})$ is the effective capacitance of the cell per unit area of attachment:

$$\Delta V_M = \alpha_{JM} V_J^\infty\left[1 - \exp\left(-\frac{t}{\tilde{\tau}_J}\right)\right], \quad (3)$$

$$\Delta V_{JM} = (\alpha_{JM} - 1)V_J^\infty\left[1 - \exp\left(-\frac{t}{\tilde{\tau}_J}\right)\right]. \quad (4)$$

Under current-clamp, the voltage change ΔV_M across the free membrane is observed with a micropipette. The polarization change ΔV_{JM} across the attached membrane follows a similar dynamics, yet with opposite sign and with a larger amplitude. Analogous exponential relations are obtained after the termination of a voltage ramp.

Onset and termination of a voltage ramp are related with capacitive current transients $I_{JM} = A_J i_{JM}$ across the attached membrane where the current density is given by Eq. 5 for $t > 0$ with a negative sign for the onset and a positive sign for the termination. E.g., the onset of a rising ramp $\Delta V_S/\Delta t_S > 0$ implies an inward current $i_{JM} < 0$ that leads to a depolarization of the free membrane, whereas its termination is related with an outward current $i_{JM} > 0$ that leads to repolarization:

$$i_{JM}(t) = \mp\tilde{c}_M\frac{c_S}{\tilde{c}_M + c_S}\frac{\Delta V_S}{\Delta t_S}\exp\left(-\frac{t}{\tilde{\tau}_J}\right). \quad (5)$$

We can achieve an instantaneous establishment and an instantaneous elimination of a stationary polarization when we superpose a positive or negative voltage step with height ΔV_S^0 to the onset and the termination of a voltage ramp, respectively. The step height must be proportional to the slope of the ramp with $\Delta V_S^0 = \pm\tilde{\tau}_J\Delta V_S/\Delta t_S$ (see Appendix).

Under voltage-clamp, there is no voltage change across the upper free membrane with $\Delta V_M = 0$. The capacitive currents through the attached membrane that originate from changes of the cleft voltage V_J are observed as pipette currents. The voltage change ΔV_{JM} and the capacitive current density i_{JM} follow Eqs. 4 and 5 when we formally set $\alpha_{JM} = 0$, also in the expressions for $\tilde{c}_M$ and $\tilde{\tau}_J$.

Gating of ion channels under voltage-clamp

A falling voltage ramp $\Delta V_S/\Delta t_S > 0$ has a depolarizing effect $\Delta V_{JM} > 0$ on the attached membrane. At a constant intracellular voltage V_M, it may activate voltage-gated ion channels in the attached membrane with ion channels in the free membrane remaining deactivated. From the current balance in the junction, we obtain Eq. 6 for the transmembrane voltage V_{JM} where V_0^i values are the reversal voltages:

$$(c_M + c_S)\frac{dV_{JM}}{dt} + \sum_i g_{JM}^i\left(V_{JM} - V_0^i\right) + g_J(V_{JM} - V_M) = -c_S\frac{dV_S}{dt}. \quad (6)$$

There is a current $I_{JM} = A_J i_{JM}$ through the attached membrane with a capacitive and an ionic component of current density according to Eq. 7:

$$i_{JM} = c_M\frac{dV_{JM}}{dt} + \sum_i g_{JM}^i\left(V_{JM} - V_0^i\right). \quad (7)$$

If the ion currents $g_{JM}^i(V_{JM} - V_0^i)$ through the attached membrane are far smaller than the leak current $g_J V_J$, they can be neglected in Eq. 6. In that case, the voltage $V_{JM}(t)$ after the onset of a voltage ramp is approximated by Eq. 4 with a time constant τ_J: A falling voltage ramp leads to a quasi-stationary depolarization of the attached membrane. That kind of extracellular voltage-clamp is able to activate ion channels in analogy to common intracellular voltage-clamp.

We may compare 1), the ionic current $I_{JM}^{ion}(t)$ through the attached membrane area A_J that is induced by a falling ramp according to Eq. 8 with the conductances $g_{JM}^i(V_{JM})$; and 2), the ionic current $I_M^{ion}(t)$ through the whole membrane area A_M that is activated by common voltage-clamp according to Eq. 9 with area-specific conductances $g_M^i(V_M)$:

$$I_{JM}^{ion} = A_J\sum_i g_{JM}^i(V_{JM})\times\left[V_{JM} - V_0^i\right], \quad (8)$$

$$I_M^{ion} = A_M\sum_i g_M^i(V_M)\times\left[V_M - V_0^i\right]. \quad (9)$$

The two currents are proportional to each other, if the depolarization ΔV_{JM} induced by a falling voltage ramp is equal to the depolarization ΔV_M applied by a pipette. Vice versa, assuming similar voltage-dependent conductances in the attached and total membrane, we can match the ionic membrane currents for extracellular and intracellular voltage-clamp when we fit the depolarization ΔV_{JM} and the area fraction $\alpha_{JM} = A_J/A_M$ of the attached membrane.

Neuronal excitation under current-clamp

Under current-clamp, rising voltage ramps have a small depolarizing effect on the free membrane whereas falling voltage ramps have a large depolarizing effect on the attached membrane due to the different serial capacitance of the two membrane domains (see Eqs. 3 and 4). Both kinds of

stimulation may activate ion channels such that an action potential is elicited.

A rising ramp $\Delta V_S/\Delta t_S > 0$ leads to a hyperpolarization of the attached membrane with $\Delta V_{JM} < 0$ such that neither Na^+ nor Ca^{2+} channels are activated. In the initial phase of stimulation, the attached membrane plays the role of a passive coupling element between capacitor and free membrane that is depolarized. When we distinguish the fast capacitive polarization and the slow dynamics of ion channels in the free membrane, we obtain Eq. 10 where the capacitive current pulse $i_{JM}^{cap}(t)$ is given by Eq. 5:

$$(A_M - A_J)\left[c_M\frac{dV_M}{dt} + \sum_i g_{FM}^i\left(V_M - V_0^i\right)\right] \approx -A_J i_{JM}^{cap}(t). \quad (10)$$

The situation resembles an intracellular stimulation by a charge pulse that is applied by a pipette. An action potential is elicited if a threshold depolarization $\Delta V_M > 0$ is reached. A relatively large slope of the rising voltage ramp is required, because the stimulating current density $i_{JM}^{cap}(t)$ is weighted by the small ratio $A_J/(A_M - A_J)$ of attached and free membrane area.

For a falling voltage ramp, the situation is quite different. The attached membrane is depolarized such that Na^+ or Ca^{2+} channels are activated there, whereas the hyperpolarized free membranes plays the role of a passive load. For the initial phase of stimulation, the dynamics is described by Eq. 11:

$$A_M c_M\frac{dV_M}{dt} + A_J\sum_i g_{JM}^i\left(V_M - V_0^i\right) \approx -A_J i_{JM}^{cap}(t). \quad (11)$$

The large capacitance may suppress the dynamics of an action potential in the small activated area of cell adhesion. Thus, we may consider a two-step mechanism of excitation: The primary depolarization of the attached membrane induces an ionic inward current. In a secondary phase, that current depolarizes the whole cell such that the initial hyperpolarization of the free membrane is overcome and an action potential is elicited in the free membrane. We describe the dynamics by Eq. 12 where the primary hyperpolarization of the free membrane is neglected and where the ionic current through the attached membrane is described by Eq. 8:

$$(A_M - A_J)\left[c_M\frac{dV_M}{dt} + \sum_i g_{FM}^i\left(V_M - V_0^i\right)\right] \approx -A_J i_{JM}^{ion}(t). \quad (12)$$

The attached membrane plays the role of an active coupling element between capacitor and free membrane that injects ionic current during the applied voltage ramp. An activation of ion channels in the attached membrane is achieved by a relatively small slope of a falling ramp. Nonetheless, it may be difficult to reach the threshold of an action potential because the stimulus current per unit area $i_{JM}^{ion}(t)$ is again weighted by the small ratio $A_J/(A_M - A_J)$ of attached and free membrane area.

RESULTS AND DISCUSSION

At first, we describe the contact of nerve cells and electrolyte/oxide/semiconductor capacitors, the displacement current through the electrolyte/oxide/semiconductor capacitors, and the passive response of nerve cells with deactivated ion channels. Subsequently, the gating of Na^+ and K^+ channels in the attached membrane is studied by capacitive stimulation with falling voltage ramps at constant intracellular voltage and their gating in the whole cell membrane by conventional variation of the intracellular voltage. Finally, action potentials are elicited under current-clamp by rising and falling voltage ramps.

Cell and capacitor

Cell-chip contact

Nerve cells with a diameter of 40–70 μm from the A-clusters of the pedal ganglia are plated in defined medium on an electrolyte/HfO_2/silicon capacitor that is coated with the peptide YIGSR, a fragment from laminin that promotes integrin-specific adhesion. Extended adhesion contacts are formed within a few hours as illustrated by Fig. 2 *A*. Electrophysiological experiments are performed around the time when the visible area of adhesion has reached the size of the cell body.

The distance between the lipid bilayer of nerve cells and the oxide is measured by fluorescence interference contrast (FLIC) microscopy using an identical procedure for cleaning

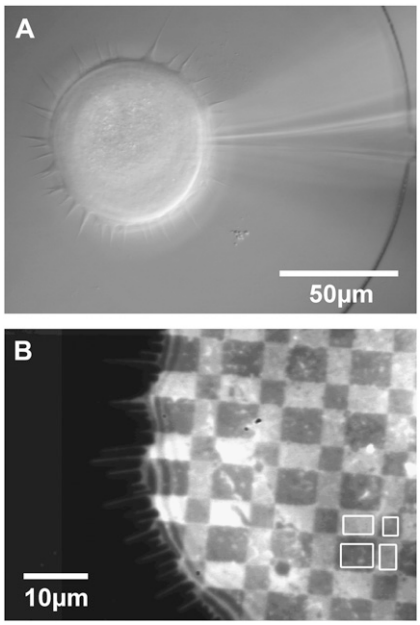

FIGURE 2 Neuron-chip system. (*A*) Differential interference contrast (DIC) micrograph of snail neuron on an electrolyte/HfO_2/silicon capacitor coated with the peptide YIGSR after 2 h in culture. The neuron forms an adhesion area that extends just beyond the cell body. (*B*) Fluorescence interference contrast (FLIC) micrograph of snail neuron stained with DiI on a silicon chip with SiO_2 terraces of four different heights. From the intensities in the marked areas, a distance of 23.5 ± 0.5 nm is evaluated between lipid membrane and chip.

and coating for the FLIC chips as for the stimulation chips. The measurements are made with a SiO_2 surface, because FLIC chips with HfO_2 are not available. Comparative measurements with HEK293 cells on TiO_2 and SiO_2 indicated that the distance does not depend on the nature of the oxide (M. H. Ulbrich and P. Fromherz, unpublished observations). A fluorescence micrograph of a neuron that was cultured for 4 h on a FLIC chip with four different terraces of SiO_2 and stained with the dye DiI is shown in Fig. 2 *B*. We observe a periodic pattern of fluorescence intensity that correlates with the height of the oxide terraces. From a fit of the intensity on four selected terraces by the FLIC theory, we obtain a distance 23.5 ± 0.5 nm between lipid bilayer and oxide. The average for $n = 11$ measurements is $d_J = 21.9 \pm 4.2$ nm.

The measured distance is lower than the value 51 ± 2 nm previously reported for snail neurons on poly-L-lysine (20). The difference may be due to the absence of growth-promoting factors in our system that adsorb to the substrate (21) and enhance the distance, or to the peptide YIGSR that may improve cell adhesion.

With an extracellular resistivity ρ_J, the distance d_J determines the sheet resistance $r_J = \rho_J/d_J$ of the cell-chip junction. For $d_J = 22$ nm, we obtain $r_J = 75$ MΩ/□, assuming a resistivity $\rho_J = 164$ MΩ cm of bulk electrolyte (22).

The estimated sheet resistance r_J is rather high due to the small distance of cell and chip. Considering the large size of the cells, the area-specific conductance $g_J = \eta_J/r_J A_J$ with contact area A_J and geometry factor η_J becomes very low. As a consequence, we expect an effective capacitive polarization of the cells according to Eqs. 3 and 4 with a stationary extracellular voltage $V_J^\infty = (c_S/g_J)\Delta V_S/\Delta t_S$ even for a relatively low capacitance c_S of the chip and moderate slopes $\Delta V_S/\Delta t_S$ of the voltage ramp.

Capacitive chip current

We determine the area-specific current i_S across an electrolyte/HfO_2/silicon capacitor without nerve cells by applying rising and falling voltage ramps above a bias voltage of $V_S = 1.5$ V with respect to a Ag/AgCl electrode. Fig. 3 shows that there is no significant direct current at the voltages $V_S = 1.5$–4V before the start of the ramps. Capacitive current appears at the onset of the ramps and disappears at their termination. There is a slow change of current during the ramps. Also, after the ramps there is a slow decay until the resting state without direct current is reached. These slow changes are due to the electronic dynamics of the heterojunction HfO_2/silicon that give rise to a capacitance that depends on voltage and frequency (10).

The current during the ramps increases with the slope of the ramps as expected for a capacitor. From the relation $i_S = c_S\, dV_S/dt$ for the current density, we estimate an average area-specific capacitance $c_S = 1.2$ μF/cm^2 in a voltage range $V_S = 1.5$–4 V. That value is in good agreement with $c_S = 1.22$ μF/cm^2 in the accumulation range of silicon at $V_S = 4$ V

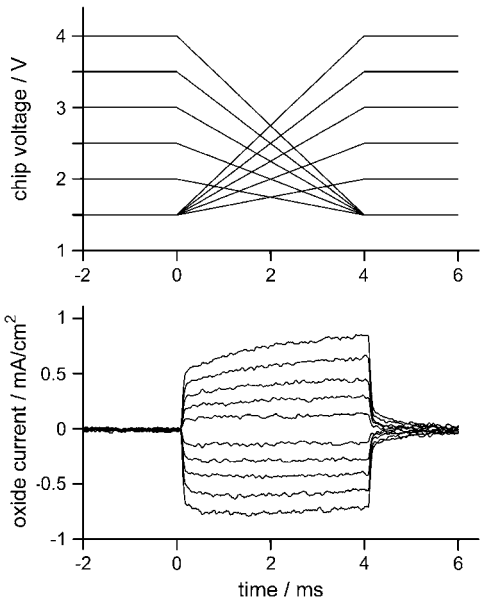

FIGURE 3 Current through HfO_2/silicon capacitor in electrolyte without cell. (*Top*) Applied voltage $V_S(t)$ of rising and falling ramps with various slopes and a duration of 4 ms. (*Bottom*) Area-specific current i_S. The current increases with the slope. The average area-specific capacitance is $\sim c_S = 1.2$ μF/cm^2 in the voltage range of $V_S = 1.5$–4 *V*. Deviations from an ideal rectangular response of capacitive current are due to the voltage and frequency dependent capacitance of the HfO_2/Si contact.

(10). The HfO_2/silicon capacitors provide four times higher densities of capacitive current than the SiO_2/silicon capacitors with $c_S = 0.3$ μF/cm^2 that were previously used for capacitive stimulation of neurons on silicon chips (12–14).

The capacitors with a diameter of 250 μm are far larger than the diameter of *Lymnaea* neurons. Thus, there is a capacitive current to the bath around the attached cells. For a current density i_S flowing through a circular electrode of radius a_S to a semi-infinite electrolyte with resistivity ρ_E, the maximum voltage drop is $V_E = i_S \rho_E a_S$ as evaluated from the Poisson equation with proper boundary conditions (23). For the highest voltage ramp $dV_S/dt = 400$ mV/ms used in this study with $a_S = 125$ μm and $\rho_E = 164$ Ωcm, the estimated voltage drop around a cell is $V_E \approx 1$ mV. Direct measurements with a patch-pipette near the capacitor are in good agreement with that prediction (data not shown). That minor voltage drop is neglected in the evaluation of our experiments in accordance with the tenets of the TDS model.

Capacitive polarization of neurons

We test the response of snail neurons to capacitive stimuli under conditions where ion channels are not activated. In the current-clamp mode of whole-cell patch-clamp, we record the change ΔV_M of the intracellular voltage, i.e., the polarization of the upper membrane. In the voltage-clamp mode, we observe the capacitive current I_{JM} through the attached

membrane. The experiments shown in Fig. 4 refer to a neuron with a contact area of $A_J = 2500\ \mu m^2$.

Passive response under current-clamp

For current-clamp experiments, we adjust the intracellular voltage to $V_M = -95$ mV and apply a rising voltage ramp to the capacitor with a slope of 100 mV/ms and a duration of 10 ms. The intracellular voltage increases within 2 ms by ~7 mV and decays within 2 ms after the ramp as shown in Fig. 4 *A* (*lowest trace*). There is a slow change during the ramp that is due to the changing capacitance of the chip as mentioned above. The dynamics of the intracellular voltage after onset and termination of a ramp is slower than the increase and decrease of the capacitive current shown in Fig. 3. It is determined by the charging and discharging of the cell-chip junction. In the TDS model, the change of intracellular voltage $\Delta V_M(t)$ is described by a single exponential according to Eq. 3. From a fit of the experiment we get a time constant $\tilde{\tau}_J \approx 0.8$ms and an amplitude $\Delta V_M^\infty \approx 7$ mV. Using the relations $\tilde{\tau}_J = (\tilde{c}_M + c_S)/g_J$ and $\Delta V_M^\infty = \alpha_{JM}(c_S/g_J)\,\Delta V_S/\Delta t_S$ with $c_S = 1.2\ \mu F/cm^2$ and $c_M = 1\ \mu F/cm^2$ (24), we derive a ratio $\alpha_{JM} = 0.15$ of attached and total membrane area and a specific conductance $g_J = 2.6\ mS/cm^2$ of the cell-chip junction.

The voltage change across the attached membrane is proportional to the voltage change across the free membrane with $\Delta V_{JM} = (1 - \alpha_{JM}^{-1})\Delta V_M$ according to Eqs. 3 and 4. From the small depolarization $\Delta V_M^\infty \approx 7$ mV and with $\alpha_{JM} = 0.15$ we evaluate a large hyperpolarizing effect $\Delta V_{JM}^\infty \approx -40$ mV in the attached membrane.

The specific conductance $g_J = \eta_J/r_J A_J$ allows us to determine the sheet resistance r_J of the cell-chip contact. From $g_J = 2.6\ mS/cm^2$ with a contact area $A_J = 2500\ \mu m^2$ estimated from a DIC micrograph, we obtain $r_J \approx 385\ M\Omega/\square$ with $\eta_J = 8\pi$. That value is five times higher than $r_J \approx 75\ M\Omega/\square$ estimated from the width of the extracellular space with bulk resistivity. We attribute the discrepancy to an enhanced resistivity ρ_J in the junction. A similar effect was observed for erythrocyte ghosts on SiO_2 coated with poly-L-lysine (29,30), whereas bulk resistivity was observed in other systems (22). The high resistivity may be related with the narrow extracellular space in our system (~20 nm) and in erythrocyte/polylysine adhesion (~10 nm), that is far smaller than for rat neurons on polylysine and HEK293 cells on fibronectin (50–70 nm) (22).

Supercharging

Extracellular and intracellular voltages are settled within the time constant of the cell-chip junction. The slow rise and decay can be accelerated by superposed voltage steps that instantaneously charge and discharge the cell-chip junction. The optimal amplitude of voltage steps ΔV_S^0 is determined

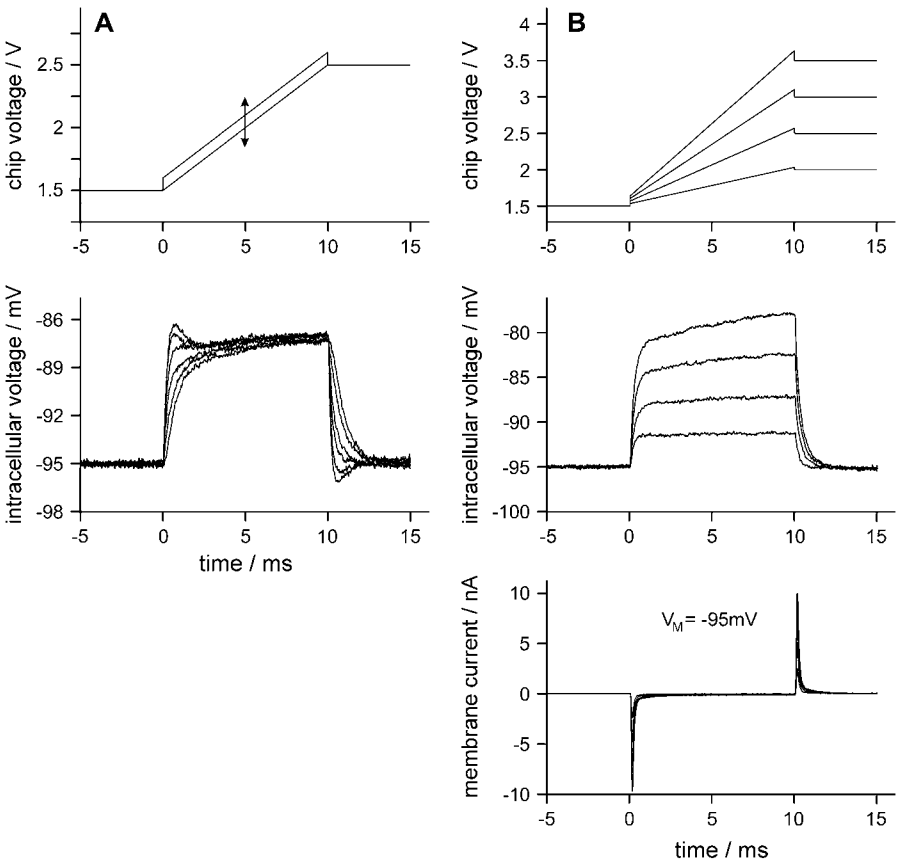

FIGURE 4 Passive response of snail neuron to capacitive stimulation with rising voltage ramps. (*A*) Current-clamp experiment starting at an intracellular voltage of −95 mV with a voltage ramp of +100 mV/ms and superposed voltage steps at the start and end of the ramp. The applied voltage (*top*) is drawn for the experiments without voltage steps and with maximum steps of ±100 mV. The current (*bottom*) is shown for all voltage steps ±0, 20,. . .100 mV. (*B*) Voltage ramps of 50, 100, 150, and 200 mV/ms with matched height of voltage steps (*top*), voltage changes in current-clamp (*center*) and currents in voltage-clamp (*bottom*).

by the slope $\Delta V_S/\Delta t_S$ of the voltage ramps with $\Delta V_S^0 = \pm \tilde{\tau}_J \Delta V_S/\Delta t_S$ (see Appendix).

Fig. 4 *A* shows current-clamp experiments for a slope of $\Delta V_S/\Delta t_S = 100$ mV/ms superposed with a set of voltage steps $\Delta V_S^0 = \pm 0, 20, \ldots, 100$ mV. A change of intracellular voltage that resembles the time course of the capacitive chip current (Fig. 3) is achieved at $\Delta V_S^0 = \pm 60$ mV. That optimum corresponds to a time constant $\tilde{\tau}_J = 0.6$ ms. When we vary the slope of the ramps in a range of 50–200 mV/ms using voltage steps $\Delta V_S^0 = 0.6\,\text{ms} \times \Delta V_S^0/\Delta t_S$ we obtain intracellular depolarizations within fractions of a millisecond as shown in Fig. 4 *B*. The empirical factor $\tilde{\tau}_J = 0.6$ ms differs from the time constant $\tilde{\tau}_J \approx 0.8$ ms of relaxation. The discrepancy is due to an intrinsic problem with the one-compartment model of the cell-chip contact to account for stationary and transient responses (see Appendix). As a consequence, the ratio of the two time constants $\tilde{\tau}_J$ reflects the ratio of the geometrical parameters η_J for stationary and transient perturbations with 0.6 ms/0.8 ms $\approx 5.78\pi/8\pi$.

Passive response under voltage-clamp

Under voltage-clamp at $V_M = -95$ mV, we measure the capacitive current through the attached membrane for a set of voltage ramps with matched voltage steps. Fig. 4 *B* shows sharp transients of membrane current at the start and termination of the ramps. They correspond to the current transients expected from Eq. 5 with an acceleration due to the superposed voltage steps. There is no current across the attached membrane during the voltage ramps. In the stationary phases, the capacitive stimulation current flows along the cell-chip junction and keeps a constant extracellular voltage.

Capacitive activation of ion channels

To study ionic currents that are induced by capacitive stimulation, we hold the cell at an intracellular voltage V_M where the channels are deactivated. The pipette current probes the current through ion channels that are opened in the attached membrane. An analogous study of capacitive activation of ion channels in the free membrane is not possible, of course. For comparison, we perform a conventional voltage-clamp experiment by variation of the intracellular voltage V_M to activate all ion channels in the free and attached membrane. In these experiments, we use an extracellular medium with blocked Ca^{2+} currents to simplify the interpretation.

Elimination of capacitive membrane current

The total current I_{JM} across the attached membrane has a capacitive and an ionic component according to Eq. 7. At first we show how the capacitive component is eliminated. In an example, we apply a falling voltage ramp with a slope of −50 mV/ms and matched supercharging steps at an intracellular voltage of −60 mV (Fig. 5 *A*). The pipette current (Fig. 5 *B*) exhibits a fast positive transient at the beginning, a slow response during the ramp and a fast negative transient at the end of the ramp. Subsequently, we hold the intracellular voltage at −120 mV. With the same stimulus, the pipette current shows again fast transients at the start and end of the ramp. The slow signal during the ramp disappears (Fig. 5 *B*).

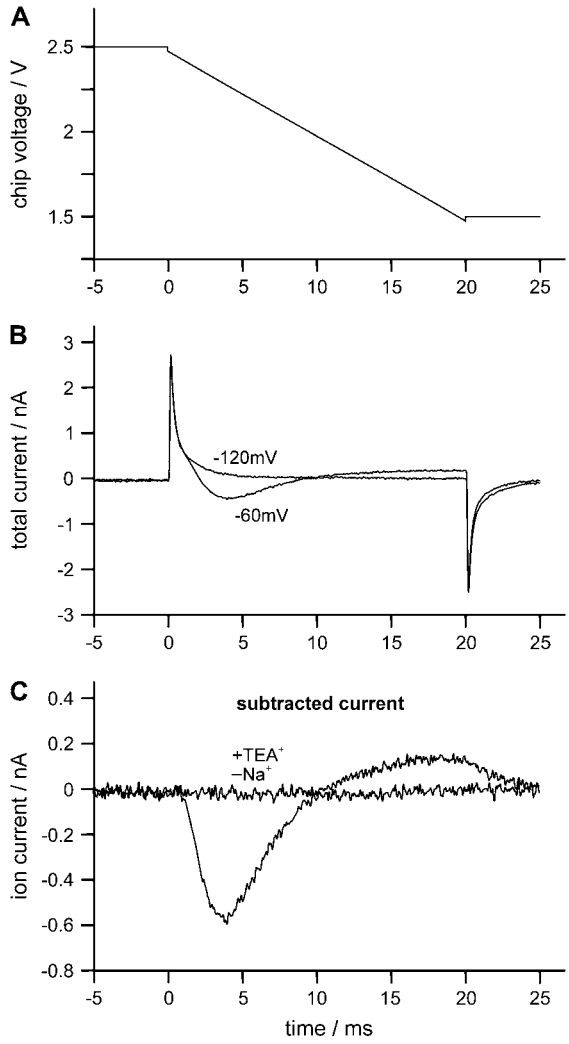

FIGURE 5 Elimination of the capacitive membrane current for extracellular stimulation under voltage-clamp. (*A*) Falling voltage ramp V_S applied to the capacitor. (*B*) Pipette current at intracellular voltages $V_M = -60$ mV and $V_M = -120$ mV in normal extracellular medium. (*C*) Net ion current obtained by subtracting the pipette currents at $V_M = -60$ mV and $V_M = -120$ mV for normal extracellular medium and for a medium with TEA^+ replacing Na^+.

We attribute the fast transients at both intracellular voltages to a capacitive current across the attached membrane. We evaluate the net ion current by subtracting the pipette current at $V_M = -120$ mV from the pipette current at $V_M = -60$ mV as shown in Fig. 5 *C*. In a control experiment, we use a bath solution that suppresses Na^+ and K^+ currents when Na^+ is replaced by Tetraethylammonium$^+$ at constant bath conductivity. With the same protocol, we find identical transients at the start and termination of the stimulation ramp at intracellular voltages of −60 mV and −120 mV (data not

shown). When we subtract the pipette signals, there is no net current left (Fig. 5 *C*). We conclude 1), that the slow signal observed in normal bath solution is due to Na^+ and K^+ currents; and 2), that the subtraction protocol in normal bath solution is able to eliminate the capacitive current. Similar results were obtained for recombinant Na^+ and K^+ channels in HEK293 cells, yet with unphysiological bath electrolytes (25,26).

Ion currents through attached and total membrane

We study the gating of ion channels in the attached membrane at an intracellular voltage of −60 mV by applying falling voltage ramps with slopes of $-20\ldots-70$ mV/ms and a duration of 20 ms. The net ion currents through the attached membrane $I_{JM}^{ion}(t)$ are shown in Fig. 6 *A*. We observe transient inward currents that become faster and shorter when the slope of the ramp is enhanced and delayed outward currents with increasing amplitudes.

For comparison, we apply a set of depolarizing intracellular voltages $\Delta V_M > 0$ starting at $V_M = -60$ mV. The whole-cell ion currents—after subtraction of capacitive and leak currents by a p/4 protocol—are depicted in Fig. 6 *B*. The response is typical for the chosen neurons from *L. stagnalis* with fast activation and inactivation of Na^+ channels and with a delayed activation of K^+ channels (27).

Apparently, the waveforms of ion current found with capacitive stimulation by falling voltage ramps closely resemble the ion currents induced by intracellular depolarization. The voltage ramps are able to activate Na^+ and K^+ channels in the attached membrane by a depolarization $\Delta V_{JM} > 0$, in analogy to the effect of depolarizing intracellular voltages $\Delta V_M > 0$ on the total membrane. The experiment implements a kind of extracellular voltage-clamp: the depolarizing voltage, $\Delta V_{JM} > 0$, is defined by the stimulation ramp according to Eq. 6 when the ionic current through the attached membrane is small compared to the current along the cell-chip junction.

However, we note some systematic differences of the current induced by extracellular as compared to intracellular voltage-clamp in Fig. 6:

1. There is a delay by ~1 ms for the initiation of Na^+ current.
2. There is a heterogeneous dynamics for the activation of Na^+ current.
3. There is no slow rise of the delayed K^+ outward current.
4. There are positive tail currents after the stimulus.

The first and fourth effect is an artifact of the amplifier: for capacitive stimulation with supercharging, we have to undercompensate the amplifier to avoid oscillations such that a constant intracellular voltage is not instantaneously established. The second effect is due to the nonuniform voltage profile in the extracellular space during a voltage ramp, a feature that is neglected in the TDS model (see Appendix). It corresponds to an imperfect space-clamping for intracellular voltage-clamp. We attribute the third effect to an enhanced

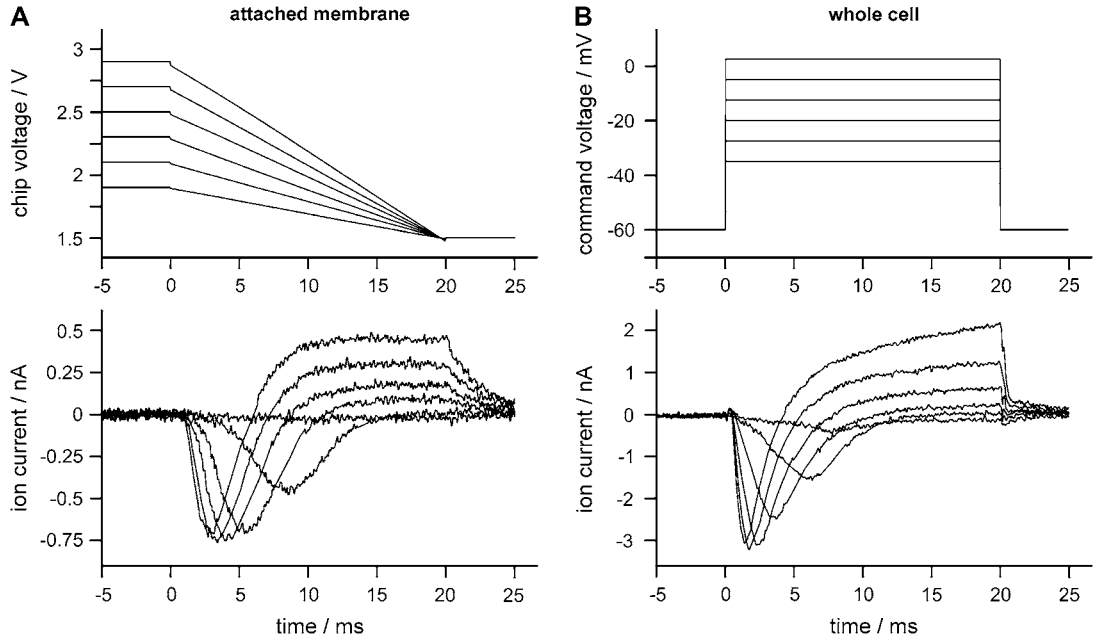

FIGURE 6 Gating of ion channels by extracellular and intracellular stimulation under voltage-clamp. (*A*) Capacitive stimulation by falling voltage-ramps with $\Delta V_S/\Delta t_S = -20, -30, \ldots -70$ mV/ms (*top*) at an intracellular voltage $V_M = -60$ mV and ion currents through the attached membrane (*bottom*). (*B*) Depolarizing pulses of intracellular voltage of $\Delta V_M = 25.0, 32.5, \ldots, 62.5$ mV starting from $V_M = -60$ mV (*top*) and ion currents through the total cell membrane (*bottom*). The two sets of currents can be matched with a voltage change across the attached membrane $\Delta V_{JM} = -1.1\ \text{ms} \times \Delta V_S/\Delta t_S$ for capacitive stimulation and a ratio $\alpha_{JM} = 0.27$ of attached and total membrane area.

K^+ concentration in the narrow extracellular cleft (28) that lowers the outward current during the ramps.

Scaling of extra and intracellular stimulation

The similar waveforms of ion currents for extracellular and intracellular stimulation indicate that the dynamics of ion conductances in attached and total membrane is similar, as described by Eqs. 8 and 9. The extracellular stimulation affects the attached membrane with ion conductances $A_J g^i_{JM}$ that are driven by the transmembrane voltage $V_{JM} = V_M - V_J$ whereas the intracellular stimulation affects the whole membrane with ion conductances $A_M g^i_{JM}$ driven by the voltage V_M.

Despite the minor difference in the waveforms, we match the two sets of measurements to get a scaling of the falling voltage ramps in terms of the transmembrane voltages with $\Delta V = -(c_S/g_J)\Delta V_S/\Delta t_S$. From a fit of the data, we obtain $c_S/g_J = 1.1$ ms and $\alpha_{JM} = 0.27$. With $c_S = 1.2\ \mu F/cm^2$, we evaluate a specific seal conductance $g_J = 1.1$ mS/cm^2. These parameters are rather similar to $\alpha_{JM} = 0.26$ and $g_J = 1.8$ mS/cm^2 that are obtained from the passive response of the same cell under current-clamp. The result shows that the concept of an ''extracellular voltage-clamp'' is adequate, i.e., that capacitive stimulation gives rise to a depolarization of the attached membrane that is determined by the slope of the ramp, the chip capacitance, and the seal conductance, and that it has the same effect on ion channels as intracellular depolarization.

Action potentials

The experiments under voltage-clamp show that voltage-gated ion channels are present in the attached and free domain of the plasma membrane, and they demonstrate an equivalence of falling voltage ramps applied to the capacitor and depolarizing pulses of intracellular voltage. Also under current-clamp, falling voltage ramps have a depolarizing effect on the attached membrane and we expect an activation of ion channels. With rising ramps, we expect that the free membrane is depolarized and that ion channels are activated there. We attempt to elicit action potentials under current-clamp using rising as well as falling voltage ramps in whole-cell patch-clamp configuration. The experiments (Figs. 7–10) are performed under the same conditions as used for voltage-clamp without Ca^{2+} currents. The results are reproducible for different cells ($n = 8$) with some variability of the threshold for action potentials.

Rising voltage ramps

Before stimulation, the intracellular voltage is adjusted to -60 ± 1 mV. Rising voltage ramps with a duration of 10 ms and with slopes of 140...190 mV/ms are applied to the capacitor starting at a bias voltage of $V_S = 1.5$ V (Fig. 7 *A*). The response of the intracellular voltage $V_M(t)$ is plotted in Fig. 7 *B*.

The weakest ramp with a slope of 140 mV/ms causes a positive change of intracellular voltage. The response saturates at $\sim\Delta V_M = 25$ mV and relaxes after the stimulus (Fig. 7 *B*, first record). It reflects the capacitive depolarization of the free membrane that is mediated by the hyperpolarized attached membrane analogous to Fig. 4. When the slope is enhanced in steps of 10 mV/ms, the passive response

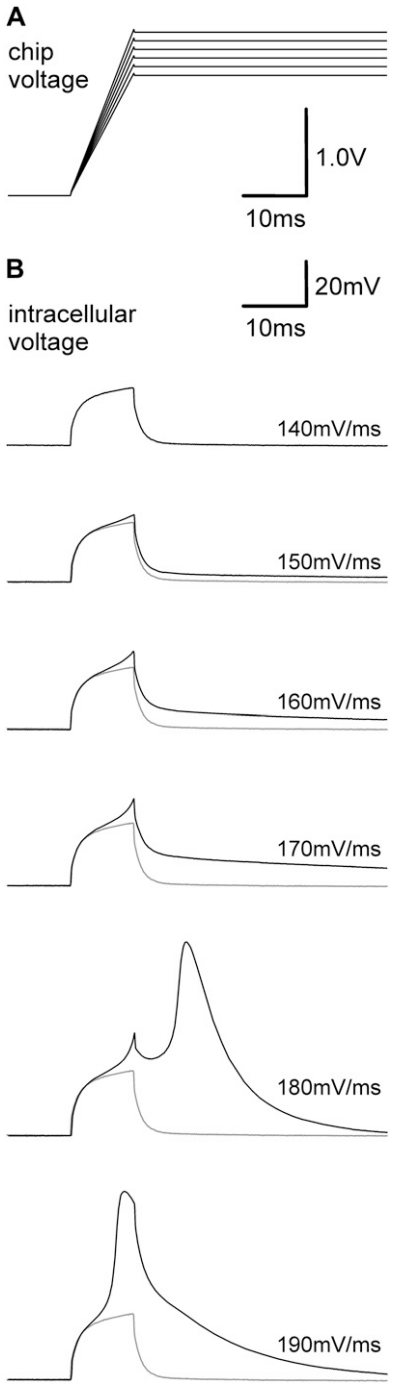

FIGURE 7 Capacitive stimulation under current-clamp with rising voltage ramps. (*A*) Applied voltage with slopes of 140,150,...,190 mV/ms. (*B*) Response of the intracellular voltage to the six different voltage ramps (*solid lines*). The shaded lines mark the passive response computed by scaling the response of the first experiment.

becomes larger. For comparison, shaded lines in Fig. 7 *B* mark the passive signals that are expected from a scaling of the first record. Superposed to the capacitive response, we observe an exponential depolarization during the ramp and a long lasting signal after the stimulus (Fig. 7 *B*, 150...170 mV/ms). Beyond a threshold of the voltage ramp, an action potential is elicited. For 180 mV/ms, the peak appears after the stimulus during the relaxing capacitive response. For 190 mV/ms, the peak is reached during the stimulus. Its decaying phase is superposed by the relaxing capacitive response.

Action potentials can be elicited by voltage ramps of different duration. The threshold of the slope is plotted in Fig. 8 versus the duration. For long stimuli, the threshold approaches a lower limit of 160 mV/ms. For shorter ramps an enhanced slope must be applied to elicit an action potential. At 2 ms duration, the slope is 400 mV/ms.

Falling voltage ramps

After adjusting the intracellular voltage to -60 ± 1 mV, falling voltage ramps with a duration of 10 ms are applied with slopes of $-25...-75$ mV/ms, ending at a bias voltage of $V_S = 1.5$ V (Fig. 9 *A*). The intracellular voltage $V_M(t)$ is plotted in Fig. 9 *B*.

For the weakest ramp with a slope of -25 mV/ms, there is a saturating response of $\Delta V_M \approx -6$ mV that relaxes after the stimulus (Fig. 9 *B*, first record). It is due to a capacitive hyperpolarization of the free membrane. When the slope of the ramp is enhanced to -35 mV/ms, the capacitive hyperpolarization increases. The responses expected from scaling of the passive signal are marked in shading. Superposed, we observe a depolarizing signal during the ramp and a long lasting signal after relaxation of the capacitive response. For larger slopes, the primary capacitive hyperpolarization changes

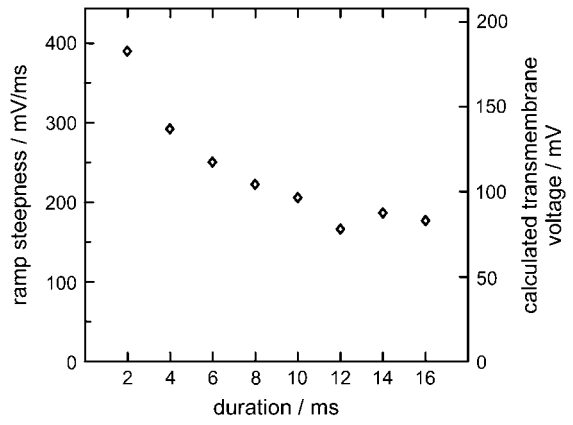

FIGURE 8 Threshold for action potentials by capacitive stimulation with rising voltage ramps. The threshold of the slope $\Delta V_S/\Delta t_S$ of voltage ramps is plotted versus the duration Δt_S of the ramps. On the right ordinate, the concomitant hyperpolarizing voltage $|V_{JM}|$ across the attached membrane is indicated as estimated from the relation $|V_{JM}| = (1-\alpha_{JM})(c_S/g_J)\Delta V_S/t_S$.

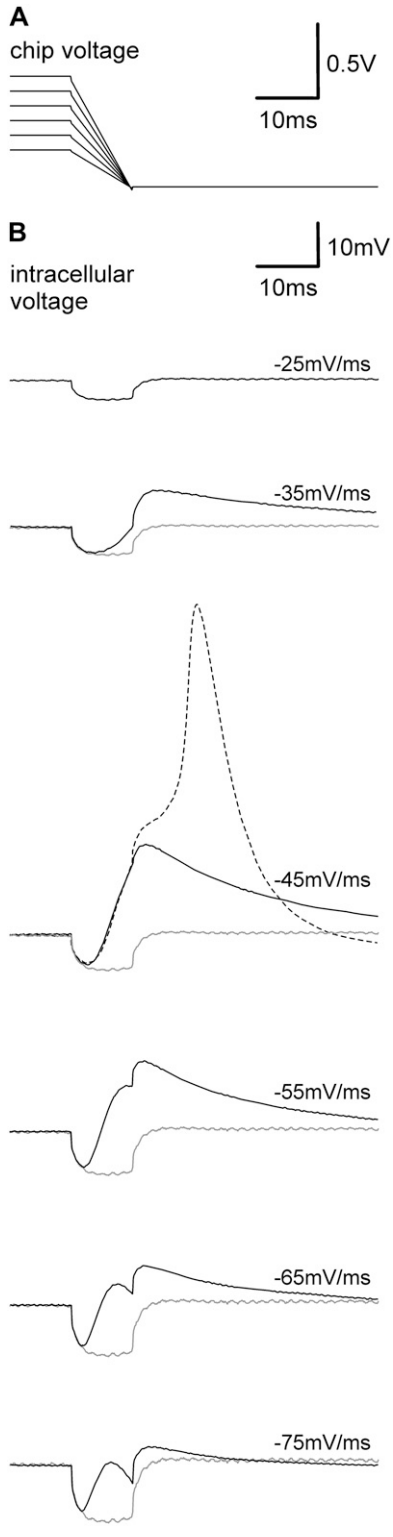

FIGURE 9 Capacitive stimulation under current-clamp with falling voltage ramps. (*A*) Applied voltages with slopes of $-25,-35,...,-75$ mV/ms. (*B*) Response of the intracellular voltage to the six different voltage ramps (*black lines*). The shaded lines mark the passive response computed by scaling the response of the first experiment. In some repetitions of the experiment, the third ramp is sometimes able to elicit an action potential (*dashed*).

to a depolarization. Sometimes it overcomes the threshold for an action potential (*dashed line* in Fig. 9 *B*, −45 mV/ms). When the slope is further enhanced, the depolarization becomes lower again (Fig. 9 *B*, −55. . .−75 mV/ms) and an action potential is not elicited.

As a measure for the efficacy of the stimuli, we evaluate the depolarization ΔV_M at the end of falling ramps from a series of experiments where no action potentials are elicited. The result is shown in Fig. 10 *A* as a contour plot obtained by interpolation. The depolarization increases and decreases with enhanced slope at a certain duration, say 10 ms, and with enhanced duration at a certain slope, say −40 mV/ms. When the ramps become shorter, an enhanced slope must be applied to achieve a certain depolarization. There exists an upper limit of depolarization that is $\sim\Delta V_M = 20$ mV in Fig. 10 *A*. The neuron is excited only if that limit is above the threshold for an action potential.

Asymmetry

The mechanism of capacitive stimulation with rising and falling ramps seems to be similar, with a mere exchange of depolarization and hyperpolarization of the attached and free membrane. However, we must point out two aspects of asymmetry:

1. There is a structural asymmetry of cell adhesion with a small area of the attached membrane and a large area of the free membrane. As a consequence, the polarizing effects on attached and free membrane have different amplitudes for a given slope of the rising or falling voltage ramp.
2. There is an asymmetry of recording. For rising and falling ramps, we probe the polarization of the free membrane.

For rising ramps, the observed voltage $V_M(t)$ reflects a primary capacitive depolarization of the free membrane and a secondary depolarization due to activated ion currents in the free membrane. For falling ramps, $V_M(t)$ indicates the primary capacitive hyperpolarization of the free membrane and a secondary depolarization that is caused by ion currents in the attached membrane.

Mechanism with rising voltage ramps

Under voltage-clamp, intracellular depolarization activates ion channels in the free membrane as shown in Fig. 6 *B*. Under current-clamp, depolarization of the free membrane is induced by a pulse of capacitive inward current at the start of a voltage ramp according to Eq. 5. Sodium channels are activated in the free membrane and the self-enhancing dynamics of an action potential is initiated as described by Eq. 10.

There is a threshold of 160 mV/ms for the slope of rising ramps in the limit of long durations (Fig. 8). With a ratio $\alpha_{JM} = 0.22$ of attached and total membrane area and a parameter $c_S/g_J = 0.6$ ms as determined for that particular cell from the passive cell response, we obtain with Eq. 3 a threshold depolarization of $\Delta V_M = 21$ mV in the limit of long durations.

When the depolarizing charge is withdrawn too early by the capacitive current pulse at the termination of the voltage ramp, the formation of the action potential is inhibited. That interference is avoided when the dynamics is accelerated by steeper ramps with enhanced inward current pulses as shown in Fig. 8. When short voltage ramps are used, attention must be paid to the danger of electroporation. Due to the smaller size, the hyperpolarization of the attached membrane is larger than the depolarization of the free membrane by a factor $\Delta V_{JM}/\Delta V_M = \alpha_{JM}^{-1} - 1$ according to Eqs. 3 and 4. With $\alpha_{JM} = 0.22$, we estimate a voltage change of $\Delta V_{JM} = 75$ mV in the limit of long ramps. For short pulses, the voltage change approaches 200 mV as indicated in Fig. 8. When long ramps are used to avoid the inhibiting effect of ramp termination, care must be taken that the voltage change across the capacitor $\Delta V_S = (\Delta V_S/\Delta t_S)\Delta t_S$ remains below the threshold of Faradayic current.

Mechanism with falling voltage ramps

Under current-clamp, falling voltage ramps depolarize the attached membrane and ion channels are activated in analogy to the voltage-clamp experiments (Fig. 6 *A*). The small area of the attached membrane has two consequences:

1. Ion channels are activated at lower slopes as compared to the effect of rising ramps on the free membrane, because

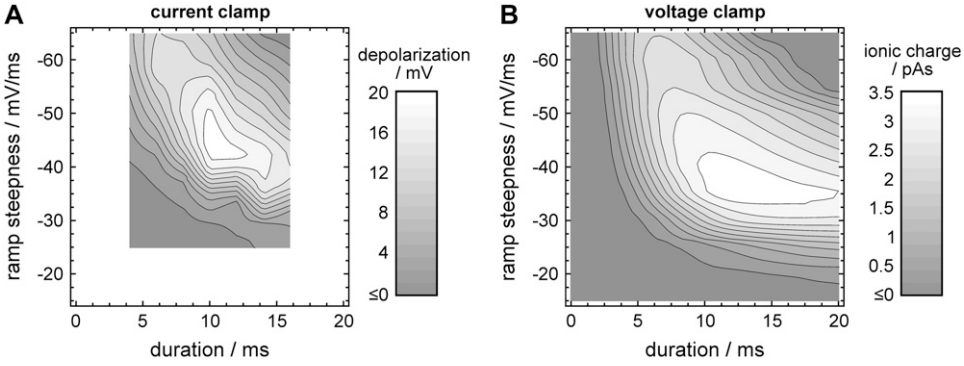

FIGURE 10 Capacitive stimulation by falling ramps. (*A*) Current-clamp. Intracellular depolarization at the end of falling voltage ramps as a function of slope and duration of the ramp. (*B*) Voltage-clamp at $V_M = -60$ mV. Injected ionic charge through attached membrane as a function of slope and stimulation time.

a larger fraction of the extracellular voltage V_J drops across the small attached membrane (see Eqs. 3 and 4). Fig. 9 *B* shows that a significant depolarizing effect appears at a slope of -35 mV/ms. Using Eq. 4 with $\alpha_{JM} = 0.26$ and $c_S/g_J = 0.7$ ms as obtained from the passive response of that particular cell (same cell as used for the voltage-clamp experiment of Fig. 6), we estimate $\Delta V_{JM} = 18$ mV.

2. In principle, an action potential may be initiated in the attached membrane by a capacitive stimulus in analogy to the effect of a rising ramp on the free membrane. However, such a local excitation is suppressed by the large capacitive load of the hyperpolarized free membrane according to Eq. 11.

The dynamics of the intracellular voltage in Fig. 9 *B* indicates a different mechanism: In a first step, the depolarization of the attached membrane activates a local inward current through activated ion channels. In a second step, that ionic current leads to a depolarization of the whole cell such that the primary capacitive hyperpolarization of the free membrane is overcome. The dynamics is described by Eq. 12. Eventually, the threshold for an action potential is reached. Such a mechanism was postulated also by Buitenweg et al. (8) based on numerical simulations. We confirm the concept of indirect ionic stimulation with falling ramps by comparing the experimental data of current-clamp and voltage-clamp.

In a first step, we evaluate the charge flow through the attached membrane under voltage-clamp (Fig. 6 *A*). For a certain slope, the injected charge increases with duration due to the Na^+ current. It decreases when the Na^+ channels inactivate and the K^+ outward current dominates. When the slope is enhanced, the charge increases due to faster activation of Na^+ channels and it decreases when the driving force for Na^+ is diminished and the K^+ outward current starts to dominate. The integrated charge injection as a function of slope and duration is shown in Fig. 10 *B* as a contour plot obtained by interpolation. There is an upper limit of injected charge at a certain duration and slope.

In a second step, we compare the injected charge under voltage-clamp with the depolarization under current-clamp as plotted in Fig. 10 *A*. The upper limit of 3.5 pAs for charge injection under voltage-clamp corresponds to the upper limit of 20 mV for depolarization. From the charge and the depolarization, we obtain a cell capacitance of 0.175 nF that corresponds to a cell diameter of 75 μm. This evaluation confirms the interpretation that the injection of ionic charge through the attached membrane determines the depolarization of the neuron with falling ramps such that eventually the threshold for an action potential is reached.

Advantages and disadvantages

For capacitive stimulation with rising as well as with falling voltage ramps, the attached membrane is a mediator between the capacitor and the excitable free membrane. With rising ramps, it promotes the injection of depolarizing capacitive current, with falling ramps the injection of depolarizing ionic current. With rising ramps, the stimulation is achieved by the charge pulse at the onset of the ramps. It is hindered for short ramps by the inverted charge pulse at the termination of the ramp. With falling ramps, the stimulation is induced by ionic charge that is injected during the whole duration of the ramp.

Neuronal stimulation by rising voltage ramps can be forced by enhancing the slope. Care must be taken, however, to avoid electroporation of the attached membrane and electrochemical reactions at the electrode when large slopes and large amplitudes are applied for weak coupling of cell and chip. In that respect, neuronal stimulation with falling ramps is more harmless because it is achieved by smaller slopes and amplitudes. However, that mechanism may completely fail to reach the threshold of an action potential if the ionic current through the attached membrane is too small due to a small area or low ion conductances in the attached membrane.

Action potentials for physiological conditions

The nature of capacitive stimulation under physiological conditions is checked for snail neurons in a common culture medium with sharp electrodes to avoid a washout of cytosolic factors that are important for Ca^{2+} currents. For each cell, we apply both rising as well as falling voltage ramps to the capacitor in a range of $\pm 25 \ldots 95$ mV/ms in steps of 10 mV/ms with a duration of 10 ms.

The response of intracellular voltage is shown in Fig. 11. Both, falling and rising voltage ramps are able to trigger action potentials with the typical Ca^{2+} shoulder of A-cluster neurons. With rising ramps (Fig. 11 *A*), we see a capacitive depolarization of the free membrane for small slopes (*traces* 1–5 in Fig. 11 *B*). Excitation is observed beyond a slope of $+75$ mV/ms. There, the action potential is elicited after relaxation of capacitive polarization. For steeper ramps the peak appears right after the onset of the ramp (*last two traces* in Fig. 11 *B*). With falling ramps (Fig. 11 *C*), we observe a hyperpolarization of the free membrane for the weakest stimulus in Fig. 11 *D*. An action potential is elicited between a slope of -35 mV/ms and -65 mV/ms. Beyond, the depolarization of the free membrane is too low again.

The crucial features of capacitive stimulation under physiological conditions are similar to the patch-clamp experiments under current-clamp. Rising voltage ramps lead to excitation above a relatively high threshold of the slope. Falling voltage ramps induce excitation at a lower threshold within a finite window of the slope. The activation of Ca^{2+} channels leads to a extended duration of inward current that assists the depolarization and lowers the threshold of excitation. As a result, capacitive stimulation is achieved for a wider range of parameters.

The efficacy of excitation under physiological conditions is checked for falling and rising ramps. While rising voltage

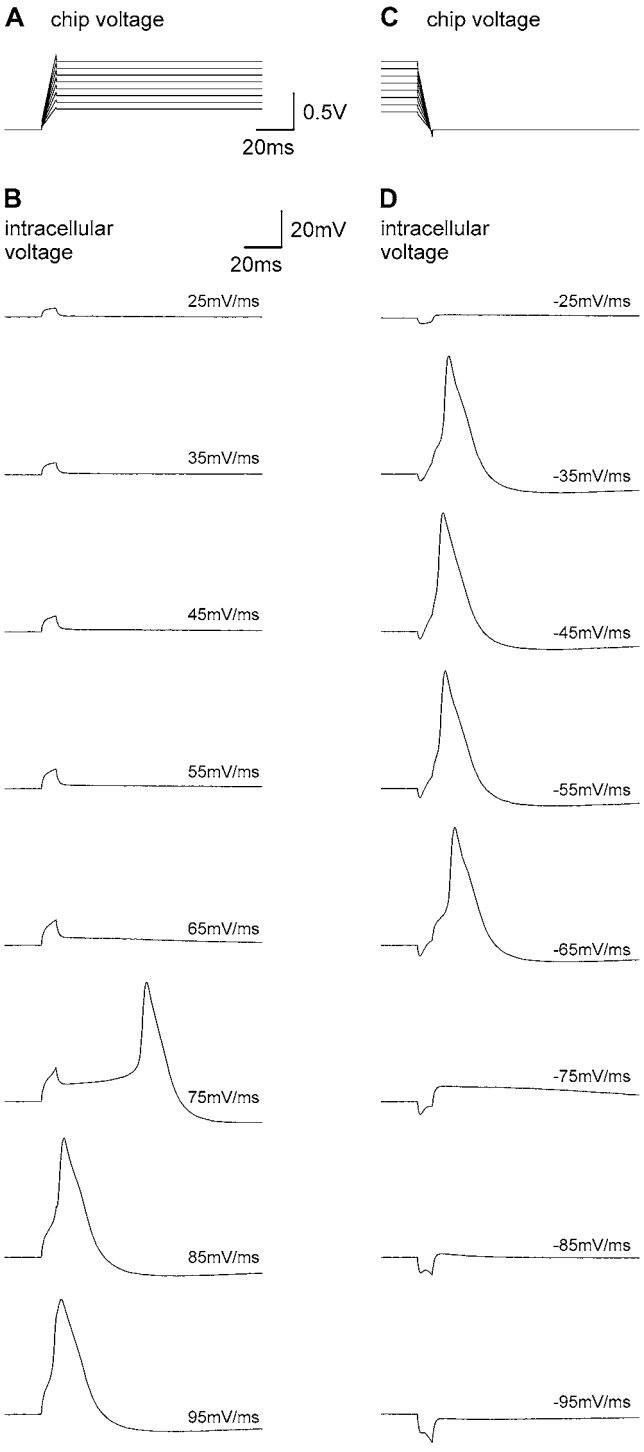

FIGURE 11 Capacitive stimulation for physiological conditions under current-clamp by rising and falling ramps with ±25,35, . . . , 95 mV/ms. (*A*) Rising voltage ramps. (*B*) Response of intracellular voltage. (*C*) Falling voltage ramps. (*D*) Response of intracellular voltage.

ramps reliably trigger action potentials, only ~30% of the cells ($n = 12$) are stimulated with falling ramps as the depolarization often is insufficient to overcome the threshold of excitation.

CONCLUSIONS

We have studied the electrophysiology of extracellular stimulation in a model system of unbranched neurons on electrolyte/oxide/silicon capacitors. Using well-defined rising and falling voltage ramps we have determined:

1. The capacitive polarization of the cells under conditions where ion channels are closed.
2. The gating of ion channels in the area of cell adhesion under voltage-clamp.
3. The elicitation of action potentials under current-clamp.

Extracellular stimulation is interpreted in terms of a two-domain-stimulation model that accounts for the polar structure of a cell/electrode system with a small membrane domain on the electrode and a larger membrane domain in contact to the bath. Two mechanism must be distinguished:

1. Rising voltage ramps depolarize the free membrane where ion channels are activated such that an action potential is elicited.
2. Falling ramps induce a depolarizing effect on the attached membrane with a current through activated ion channels that depolarizes the free membrane such that an action potential is triggered.

With falling ramps, stimulation may fail because the ion current through the attached membrane is not necessarily sufficient to elicit an action potential. Excitation can be always achieved by rising voltage ramps with a sufficiently high slope. In that case, however, the danger of electroporation and Faradayic current must be taken into account.

The stimulation of a large and unbranched nerve cell by an ideal capacitor and its interpretation with a two-domain-stimulation model may serve as a basis for the understanding and optimization of extracellular stimulation in other situations:

1. All aspects of the analysis remain valid for planar metal electrodes and also for photoconductive stimulation (31, 32). The application of anodic and cathodic current pulses corresponds to rising and falling voltage ramps. However, care must be taken in these systems to avoid toxic effects by the Faradayic currents.
2. With mammalian neurons, the stimulation will be more difficult because both the sheet resistance r_J and the area A_J of the cell-chip contact are smaller than for snail neurons (22,33). When a voltage ramp with an enhanced slope is applied for compensation of the weaker chip-cell interaction, the duration of the stimulus must be shortened to avoid Faradayic current.
3. For arborized neurons, the assignments of attached and free domain of the cell membrane on an electrode demand special attention.
4. For brain tissue, we may take the dynamics of the model system as a starting point. However, a prerequisite for an elucidation of extracellular stimulation is an analysis of the

microscopic structure of the tissue/electrode contact region. If the contact between individual neurons and an electrode is weak, rather large capacitive currents are required with the danger of electroporation and Faradayic current.

APPENDIX

One-compartment model and core-coat conductor model

Current conservation in the planar core-coat conductor of a cell-capacitor junction is expressed by Eq. A1 at constant intracellular voltage V_M without ion conductances in the cell membrane (18). V_J is the extracellular voltage, V_S is the voltage of the substrate, c_M and c_S are the area-specific capacitances of membrane and substrate and r_J is a homogeneous sheet resistance:

$$(c_M + c_S)\frac{\partial V_J}{\partial t} - \frac{1}{r_J}\nabla^2 V_J = c_S\frac{dV_S}{dt}. \tag{A1}$$

In a one-compartment model (Fig. 1 *B*), current conservation per unit area is expressed by Eq. A2 with a representative extracellular voltage V_J with respect to the bath on ground and with an area-specific conductance g_J of the junction:

$$(c_S + c_M)\frac{dV_J}{dt} + g_J V_J = c_S\frac{dV_S}{dt}. \tag{A2}$$

A match of the one-compartment model to the core-coat conductor model is defined by a substitution $-r_J^{-1}\nabla^2 V_J \Rightarrow g_J V_J$ (14). In stimulation experiments, we observe the response of a cell to the interaction of a capacitor with the whole attached membrane. To obtain a matching, we compare the representative voltage of the one-compartment model with the spatially averaged voltage of the core-coat conductor. Considering the physical dimensions, we must look for a relation $g_J = \eta_J/(r_J A_J)$ with the area A_J of the junction and a dimensionless factor η_J.

Voltage ramp

We consider a stationary voltage ramp $dV_S/dt = \Delta V_S/\Delta t_S$ that is applied to the capacitor. The stationary profile $V_J^\infty(a)$ of extracellular voltage along a radius coordinate a of a circular contact is given by Eq. A3 and the average voltage by Eq. A4 where a_J is the radius of a contact with area $A_J = a_J^2\pi$. For the same voltage ramp, the representative extracellular voltage of the one-compartment model is given by Eq. A5:

$$V_J^\infty(a) = \left(1 - \frac{a^2}{a_J^2}\right)\frac{A_J r_J c_S \Delta V_S}{4\pi \quad \Delta t_S}, \tag{A3}$$

$$\langle V_J^\infty \rangle = \frac{A_J r_J c_S}{8\pi}\frac{\Delta V_S}{\Delta t_S}, \tag{A4}$$

$$V_J^\infty = \frac{c_S}{g_J}\frac{\Delta V_S}{\Delta t_S}. \tag{A5}$$

When we identify the averaged voltage profile of Eq. A4 with the representative voltage of Eq. A5, we obtain the relation $g_J = 8\pi/A_J r_J$ with $\eta_J = 8\pi$. That matching of the one-compartment model is suitable to account for the stationary features of a cell-chip contact.

Voltage step

When a voltage step ΔV_S^0 is applied to the whole area of the capacitor at time $t = 0$, a pulse $c_S\Delta V_S^0\delta(t)$ of displacement current is injected into the junction per unit area. The extracellular voltage in a circular contact $V_J(a,t)$ can be expressed by a series of exponentials according to Eq. A6 with the time constants τ_n where x_n is the n^{th} zero of the Bessel function J_0 (23,34),

$$V_J(a,t) = \frac{c_S\Delta V_S^0}{c_M + c_S}\sum_{n=1}^{\infty}\frac{2J_0(x_n a/a_J)}{x_n J_1(x_n)}\exp(-t/\tau_n)$$

$$\tau_n = \frac{(c_S + c_M)r_J a_J^2}{x_n^2}. \tag{A6}$$

At time $t = 0$, the voltage is constant across the junction. The initial situation rapidly changes to a voltage profile that is described by the Bessel function J_0. That profile decays in a slower relaxation process. In our system, the two pertinent time constants are typically in a range of $\tau_2 \approx 0.1$ ms and $\tau_2 \approx 0.5$ ms.

For the average extracellular voltage we obtain Eq. A7. The transient extracellular voltage in the one-compartment model is a single exponential with the time constant τ_J according to Eq. A8:

$$\langle V_J \rangle = \frac{c_S\Delta V_S^0}{c_M + c_S}\sum_{n=1}^{\infty}\frac{4}{x_n^2}\exp(-t/\tau_n), \tag{A7}$$

$$V_J = \frac{c_S\Delta V_S^0}{c_M + c_S}\exp(-t/\tau_J),\ \tau_J = \frac{c_S + c_M}{g_J}. \tag{A8}$$

When we identify the time constant τ_1 of the core-coat conductor with the time constant τ_J of the one-compartment model, we obtain the relation $g_J = 5.78\pi/A_J r_J$ with $\eta_J = 5.78\pi$. That matching of the one-compartment model is suitable to account for the dynamical features of a cell-chip contact (28).

Dynamics and supercharging

The dynamics of the voltage profile becomes more involved when a voltage ramp is applied for $t > 0$, or when a voltage ramp and a voltage step are superposed. We do not consider these details of the core-coat conductor here. In the one-compartment model, the extracellular voltage relaxes for a voltage ramp starting at $t = 0$ according to Eq. A9:

$$V_J = \tau_J\frac{c_S}{c_M + c_S}\frac{\Delta V_S}{\Delta t_S}\left[1 - \exp\left(-\frac{t}{\tau_J}\right)\right]. \tag{A9}$$

The stationary voltage as well as the dynamics depend on the same time constant $\tau_J = (c_M + c_S)/g_J$. Apparently, a consistent match to the complete dynamics is not possible, considering the different geometrical factors $\eta_J = 8\pi$ and $\eta_J = 5.78\pi$ that are used to choose g_J and τ_J for a stationary perturbation and for relaxation.

In the one-compartment model, an instantaneous establishment of a stationary extracellular voltage V_J at a time $t = 0$ can be attained when a superposition of a voltage ramp and a voltage step is applied. When we insert the Ansatz $V_J(t) = V_J^0\Theta(t)$ into Eq. A2 and integrate, we obtain Eq. A10 with the Heaviside function $\Theta(t)$:

$$V_S = V_J^0\frac{c_M + c_S}{c_S}\left[\Theta(t) + \frac{1}{\tau_J}t\right]. \tag{A10}$$

Equation A10 implies the relation $\Delta V_S^0 = \tau_J\Delta V_S/\Delta t_S$ between the height of the step and the slope of the ramp. It leads to a perfect compensation of the relaxation dynamics due to a voltage ramp (Eq. A9) by the exponential response to a voltage step (Eq. A8). In practice, however, such a perfect compensation is not achieved because an optimal match of one-compartment model and of core-coat conductor requires different time constants τ_J with different factors η_J for the stationary level and for the dynamics.

We thank Frank Wallrapp for the chips, Alexander Kaul and Ralf Zeitler for help with cell culture, and Moritz Voelker for critical reading of the manuscript.

The project was supported by the Deutsche Forschungsgemeinschaft (grant No. SFB 563) and the European Union (grant No. IST-2001-38915).

REFERENCES

1. Garcia, L., G. D'Alessandro, B. Bioulac, and C. Hammond. 2005. High-frequency stimulation in Parkinson's disease: more or less? *Trends Neurosci.* 28:209–216.
2. Merabet, L. B., J. F. Rizzo, A. Amedi, D. C. Somers, and A. Pascual-Leone. 2005. What blindness can tell us about seeing again: merging neuroplasticity and neuroprosthesis. *Nat. Rev. Neurosci.* 6:71–77.
3. Huang, C. Q., R. K. Shepherd, P. M. Seligman, and G. M. Clark. 1998. Reduction in excitability of the auditory nerve following acute electrical stimulation at high stimulus rates: III. Capacitive versus non-capacitive coupling of the stimulating electrodes. *Hear. Res.* 116: 55–64.
4. Ranck, J. B. 1975. Which elements are excited in electrical stimulation of mammalian central nervous system: a review. *Brain Res.* 98: 417–440.
5. McIntyre, C. C., and W. M. Grill. 1999. Excitation of central nervous system neurons by nonuniform electric fields. *Biophys. J.* 76:878–888.
6. Jimbo, Y., and A. Kawana. 1993. Electrical stimulation and recording from cultured neurons using a planar electrode array. *Bioelectrochem. Bioenerg.* 29:193–204.
7. Maher, P. M., J. Pine, J. Wright, and Y. C. Tai. 1999. The neurochip: a new multielectrode device for stimulating and recording from cultured neurons. *J. Neurosci. Method.* 87:45–56.
8. Buitenweg, J. R., W. L. C. Rutten, and E. Marani. 2002. Extracellular stimulation window explained by a geometry-based model of the neuron-electrolyte contact. *IEEE Trans. Biomed. Eng.* 49:1591–1599.
9. Wagenaar, D. A., J. Pine, and S. M. Potter. 2004. Effective parameters for stimulation of dissociated cultures using multi-electrode arrays. *J. Neurosci. Method.* 138:27–37.
10. Wallrapp, F., and P. Fromherz. 2006. TiO_2 and HfO_2 in electrolyte-oxide-silicon configuration for applications in bioelectronics. *J. Appl. Phys.* 99:114103.
11. Maria, J.-P. 2005. Alternative dielectrics for silicon-based transistors. *In* High Dielectric Constant Materials. H. R. Huff and D. C. Gilmer, editors. Springer, Berlin. 223–251.
12. Fromherz, P., and A. Stett. 1995. Silicon-neuron junction: capacitive stimulation of an individual neuron on a silicon chip. *Phys. Rev. Lett.* 75:1670–1673.
13. Jenkner, M., B. Mueller, and P. Fromherz. 2001. Interfacing a silicon chip to pairs of snail neurons connected by electrical synapses. *Biol. Cybern.* 84:230–249.
14. Fromherz, P. 2005. The neuron-semiconductor interface. *In* Bioelectronics, from Theory to Application. I. Willner and E. Katz, editors. Wiley-VCH, Weinheim. 339–394.
15. Syed, N. I., H. Zaidi, and P. Lovell. 1999. In vitro reconstruction of neuronal circuits: a simple model system approach. *In* Modern Techniques in Neuroscience Research. U. Windhorst and H. Johansson, editors. Springer, Berlin, Heidelberg. 361–377.
16. Iwamoto, Y., F. A. Robey, J. Graf, M. Sasaki, H. K. Kleinman, Y. Yamada, and G. R. Martin. 1987. YIGSR, a synthetic pentapeptide, inhibits experimental metastasis formation. *Science.* 238:1132–1134.
17. Lambacher, A., and P. Fromherz. 2002. Luminescence of dye molecules on oxidized silicon and fluorescence interference contrast microscopy of biomembranes. *J. Opt. Soc. Am. B.* 19:1435–1453.
18. Weis, R., and P. Fromherz. 1997. Frequency dependent signal-transfer in neuron-transistors. *Phys. Rev. E.* 55:877–889.
19. Regehr, W. G., J. Pine, C. S. Cohan, M. D. Mischke, and D. W. Tank. 1989. Sealing cultured invertebrate neurons to embedded dish electrodes facilitates long-term stimulation and recording. *J. Neurosci. Method.* 30:91–106.
20. Zeck, G., and P. Fromherz. 2003. Repulsion and attraction by extracellular matrix protein in cell adhesion studied with nerve cells and lipid vesicles on silicon chips. *Langmuir.* 19:1580–1585.
21. Wong, R. G., R. D. Hadley, S. B. Kater, and G. C. Hauser. 1981. Neurite outgrowth in molluscan organ and cell culture: the role of conditioning factor(s). *J. Neurosci.* 1:1008–1021.
22. Gleixner, R., and P. Fromherz. 2006. The extracellular electrical resistivity in cell adhesion. *Biophys. J.* 90:2600–2611.
23. Carslaw, H. S., and J. C. Jaeger. 1959. Conduction of Heat in Solids, 2nd Ed. Clarendon Press, Oxford. 214–216.
24. Wan, X., J. A. Harris, and C. E. Morris. 1995. Responses of neurons to extreme osmomechanical stress. *J. Membr. Biol.* 145:21–31.
25. Ulbrich, M. H., and P. Fromherz. 2005. Opening of K^+ channels by capacitive stimulation from silicon chip. *Appl. Phys. A.* 81:887–891.
26. Schoen, I., and P. Fromherz. 2005. Activation of Na^+ channels in cell membrane by capacitive stimulation with silicon chip. *Appl. Phys. Lett.* 87:193901.
27. Staras, K., J. Gyori, and G. Kemenes. 2002. Voltage-gated ionic currents in an identified modulatory cell type controlling molluscan feeding. *Eur. J. Neurosci.* 15:109–119.
28. Brittinger, M., and P. Fromherz. 2005. Field-effect transistor with recombinant potassium channels: fast and slow response by electrical and chemical interactions. *Appl. Phys. A.* 81:439–447.
29. Kiessling, V., B. Mueller, and P. Fromherz. 2000. Extracellular resistance in cell adhesion measured with a transistor probe. *Langmuir.* 16:3517–3521.
30. Braun, D., and P. Fromherz. 2004. Imaging neuronal seal resistance on silicon chip using fluorescent voltage-sensitive dye. *Biophys. J.* 87: 1351–1359.
31. Goda, Y., and M. A. Colicos. 2006. Photoconductive stimulation of neurons cultured on silicon wafers. *Nature Protocols.* 1:461–467.
32. Starovoytov, A., J. Choi, and H. S. Seung. 2005. Light-directed electrical stimulation of neurons cultured on silicon wafers. *J. Neurophysiol.* 93:1090–1098.
33. Voelker, M., and P. Fromherz. 2005. Signal transmission from individual mammalian nerve cell to field-effect transistor. *Small.* 1: 206–210.
34. Crank, J. 1975. The Mathematics of Diffusion, 2nd Ed. Oxford University Press, Oxford. 73–74.